Constant-Q wavelet estimation via a nonstationary Gabor spectral model

Jeff P. Grossman, Gary F. Margrave, Michael P. Lamoureux, and Rita Aggarwala

ABSTRACT

As a seismic wave propagates through the earth, its amplitude attenuates over time and frequency due to microscopic processes such as internal friction. Thus, on one hand, the earth is an anelastic medium; on the other hand, Hooke's law, which is normally used in the derivation of the wave equation, applies only to perfectly elastic media. Despite that fact, seismic attenuation can be modelled macroscopically over typical seismic bandwidths via an exponential amplitude decay in both time and frequency, at a rate determined by a single dimensionless quantity, *Q*.

Current seismic deconvolution methods, based on the stationary convolutional model, attempt to estimate, and subsequently filter out, the embedded causal wavelet. We present a nonstationary seismic model, expressed in the time-frequency Gabor domain, in which (1) the embedded causal wavelet is represented as the product of a stationary seismic signature with a nonstationary exponential decay; and (2) a nonstationary impulse response for the earth is tractable.

By least-squares fitting our model to the Gabor-transformed seismic trace, we robustly determine both a unique Q-value and an estimate of the seismic signature, and thus an estimate of the nonstationary causal wavelet. Using these estimates to obtain a smoothed version of the seismic trace in the time-frequency domain, a least squares nonstationary minimum phase deconvolution filter is constructed. The preliminary results, coded in MATLAB®, look very promising. It is hoped that in future work, the residual error in this least-squares approximation will provide a good measure of the ambient random noise, up to the accuracy of our model, and hence a method by which to improve the signal-to-noise ratio.

INTRODUCTION

This paper is concerned with the application of Gabor theory to the analysis, modelling, and subsequent deconvolution of a nonstationary, constant-Q-attenuated seismic signal. In a broader context, Gabor deconvolution is discussed by Margrave and Lamoureux (2001). The Gabor theory sets the stage for *nonstationary analysis* of a signal, "in which time and frequency play symmetrical parts, and which contains 'time analysis' and 'frequency analysis' as special cases." (Gabor, 1946) Indeed, our everyday experience with sound, as in speech or music, demands a mathematical description that places time and frequency analysis on equal footings. The human ear, which operates much like a hydrophone in principle, combined with the brain's processing capabilities, deciphers band-limited acoustic amplitude information into temporally localized packets of spectral information. Conversely, while following a prescribed musical score, a musician transforms a time-frequency representation of a signal into temporally varying acoustic amplitude data.

The Fourier theory, although mathematically sound, is an idealized theory: it fails to capture our intuition that "frequency content" changes with time. "The reason is that the Fourier-integral method considers phenomena in an infinite interval, …and this is very far from our everyday point of view."(Gabor, 1946) These fundamental observations strongly suggest that we ought to be modelling the localized time and frequency characteristics of a seismic signal simultaneously; and it is the milestone theory of Gabor that can provide us with the appropriate mathematical tools.

We first present a derivation, to first order, of a time-variant spectral model for the Gabor transform of a constant-Q-attenuated seismic trace. Remarkably, in addition to being intuitively plausible, this model expresses a generalization of the familiar *convolutional model* (as described in Sheriff and Geldart, 1982, for example). Next, the model is fitted to the data in the least squares sense. This process provides estimates for both Q and the stationary part of the wavelet, and thus an estimate of the nonstationary, Q-attenuated wavelet. The theory is then used to formulate an algorithm for the deconvolution of a synthetic Q-attenuated seismic trace. Finally, we close with an illustrative discussion of our preliminary results.

A TIME-VARIANT SPECTRAL MODEL

Let $r(t)$ be a (random) reflectivity, $w(t)$ a stationary wavelet, and $\alpha(t,f)$ the time-frequency symbol of a constant Q operator. Specifically for the latter

$$\alpha(t,f) = e^{-\pi f t/Q - iH(\pi f t/Q)}, \tag{1}$$

where *H* denotes the Hilbert transform. A stationary wavelet, in this context, is a wavelet whose time-frequency decomposition is equivalent to its Fourier transform, which in turn depends only on frequency. An assumption is that this Fourier transform, $\hat{w}(f)$, is smooth. Note that by definition $\alpha(t,f)$ is also reasonably smooth.

Then a nonstationary synthetic can be constructed by a nonstationary convolution (see Margrave, 1998, or Margrave and Ferguson, 1998) of the Q operator and the reflectivity, followed by a stationary convolution with the wavelet. Letting $s(t)$ denote the nonstationary synthetic trace, then using the mixed domain form of nonstationary convolution (Margrave, 1998, or Margrave and Ferguson, 1998) gives

$$\hat{s}(f) = \hat{w}(f) \int_{-\infty}^{\infty} \alpha(t,f) r(t) e^{-2\pi i f t} dt, \tag{2}$$

where the hat denotes the Fourier transform. Thus

$$\begin{aligned} s(t) &= \int_{-\infty}^{\infty} \hat{w}(f)\left[\int_{-\infty}^{\infty} \alpha(u,f) r(u) e^{-2\pi i f u} du\right] e^{2\pi i f t} df \\ &= \iint \hat{w}(f)\alpha(u,f) r(u) e^{2\pi i f [t-u]} df du. \end{aligned} \tag{3}$$

This may seem a bit lacking in justification but is, in fact, quite well established. We now want to show that a time-frequency decomposition of $s(t)$, call it $Ts(\tau,\nu)$, has the approximate factorization: $Ts(\tau,\nu) \sim \hat{w}(\nu)\alpha(\tau,\nu)Tr(\tau,\nu)$. Here $Tr(\tau,\nu)$ is the time-frequency decomposition of the reflectivity. This will be demonstrated using Gabor spectra as the time-frequency decomposition (see e.g., Margrave and Lamoureux, 2001 for a related treatment, or Feichtinger and Strohmer, 1998 for a thorough treatment of Gabor analysis).

Now, the Gabor transform of $s(t)$ is defined as

$$V_g s(\tau,\nu) = \int_{-\infty}^{\infty} s(t) g(t-\tau) e^{-2\pi i \nu t} dt, \tag{4}$$

where $g(t)$ is the Gabor analysis window (usually a Gaussian). Substituting (3) into (4) gives

$$V_g s(\tau,\nu) = \int_{-\infty}^{\infty} \left[\iint \hat{w}(f)\alpha(u,f) r(u) e^{2\pi i f [t-u]} df du\right] g(t-\tau) e^{-2\pi i \nu t} dt. \tag{5}$$

Consider the *t* integral in equation (5):

$$I = \int g(t-\tau) e^{-2\pi i t[\nu - f]} dt. \tag{6}$$

Let $t' = t - \tau$ and so

$$I = \int g(t') e^{-2\pi i [t'+\tau][\nu - f]} dt' = e^{-2\pi i \tau [\nu - f]} \hat{g}(\nu - f), \tag{7}$$

so that equation (5) becomes

$$V_g s(\tau,\nu) = \iint \hat{w}(f)\alpha(u,f) r(u) e^{-2\pi i f u} e^{-2\pi i \tau [\nu - f]} \hat{g}(\nu - f) df du. \tag{8}$$

Now, let $f' = \nu - f$ so that

$$V_g s(\tau,\nu) = \iint \hat{w}(\nu - f')\alpha(u,\nu - f') r(u) e^{-2\pi i [\nu - f'] u} e^{-2\pi i \tau f'} \hat{g}(f') df' du. \tag{9}$$

Then, using Taylor series' to represent $\hat{w}(\nu - f')$ and $\alpha(u,\nu - f')$,

$$V_g s(\tau,\nu) = \iint \left[\hat{w}(\nu) - f' \frac{\partial \hat{w}}{\partial \nu}(\nu) + \ldots \right] \bullet$$

$$\left[\alpha(u,\nu) - f' \frac{\partial \alpha}{\partial \nu}(u,\nu) + \ldots \right] r(u) e^{-2\pi i[\nu - f']u} e^{-2\pi i \tau f'} \hat{g}(f') df' du \tag{10}$$

or

$$V_g s(\tau,\nu) = \hat{w}(\nu) \int \alpha(u,\nu) r(u) e^{-2\pi i \nu u} \left[\int e^{2\pi i[u-\tau]f'} \hat{g}(f') df' \right] du + \cdots \tag{11}$$

or

$$V_g s(\tau,\nu) = \hat{w}(\nu) \int \alpha(u,\nu) r(u) g(\tau - u) e^{-2\pi i \nu u} du + \cdots. \tag{12}$$

Let $u' = \tau - u$:

$$V_g s(\tau,\nu) = \hat{w}(\nu) \int \alpha(\tau - u',\nu) r(\tau - u') g(u') e^{-2\pi i \nu [\tau - u']} du' + \cdots \tag{13}$$

Expand $\alpha(\tau - u',\nu)$ in a Taylor series:

$$V_g s(\tau,\nu) = \hat{w}(\nu) \alpha(\tau,\nu) \int r(\tau - u') g(u') e^{-2\pi i \nu [\tau - u']} du' + \cdots \tag{14}$$

Now, back to $u = \tau - u'$

$$V_g s(\tau,\nu) = \hat{w}(\nu) \alpha(\tau,\nu) \int r(u) g(\tau - u) e^{-2\pi i \nu u} du + \cdots \tag{15}$$

or

$$V_g s(\tau,\nu) = \hat{w}(\nu) \alpha(\tau,\nu) V_g r(\tau,\nu) + \cdots. \tag{16}$$

These last several manipulations seem almost circular but they amount to a justification that $\alpha(u,v)$ can be pulled out of the integral in equation (12), where it becomes $\alpha(\tau,v)$. This analysis shows that the leading order behaviour fits the nonstationary model but so far provides no estimate of the next asymptotic term.

DISCUSSSION OF THE PROBLEM

To first order, the Gabor-spectral model from equation (16) is

$$\left| V_g s(\tau,\nu) \right| = \left| \hat{w}(\nu) \right| \left| \alpha(\tau,\nu) \right| \left| V_g r(\tau,\nu) \right|. \tag{17}$$

where we have chosen to work with the magnitudes of the various complex quantities and the vertical bars denote absolute values. The left side of (17) is the only known quantity, namely the Gabor transform of the seismic trace. It is assumed that the

reflectivity is approximately white and so its Gabor transform is effectively treated as the residual error term in the-least squares estimation process.

The unknowns in (17) are the seismic signature's spectrum, $\hat{w}(\nu)$, and the value of Q in the time-frequency symbol of the Q-operator, $\alpha(\tau,\nu)$. Of course, the reflectivity, $V_g r(\tau,\nu)$, is also unknown: it characterizes the very subsurface geology that we ultimately want to determine. However, once $|\hat{w}(\nu)|$ and $|\alpha(\tau,\nu)|$ have been estimated, their product represents a smoothed version of $|V_g s(\tau,\nu)|$, and it is then a straightforward matter to design a nonstationary minimum phase deconvolution filter.

The first goal is to obtain estimates of Q and the function $\hat{w}(\nu)$ that satisfy (17) in the least-squares sense.

SOLUTION OF THE LEAST SQUARES PROBLEM

We now assume that the Gabor transform of the reflectivity, $|V_g r(\tau,\nu)|$, is "white" with a mean of unity. Precisely what is meant here by "white" is not easily defined but, intuitively, we mean that $|\hat{w}(\nu)||\alpha(\tau,\nu)|$ provides the general shape of $|V_g s(\tau,\nu)|$ while $|V_g r(\tau,\nu)|$ provides only detail. Thus we will drop the $|V_g r(\tau,\nu)|$ term from equation (17) and seek a trace model as

$$S(\tau,\nu) = W(\nu) e^{-\pi\nu\tau/Q}, \tag{18}$$

where $S = |V_g s|$, $W = |\hat{w}|$, and $e^{-\pi\nu\tau/Q} = |\alpha(\tau,\nu)|$. The equality in (18) is interpreted in the least-squares sense meaning that a residual error with minimized L^2 norm is assumed. The residual error represents the random ambient noise plus the Gabor transform of the reflectivity. A further simplification is obtained by considering the natural logarithm of both sides of (18), which effectively removes the exponential term:

$$\ln S(\tau,\nu) = \ln\left[W(\nu)\right] - \pi\tau\nu/Q. \tag{19}$$

Step one: least squares estimate of *Q* in terms of *W*

We first minimize the function $\alpha = \alpha(W,Q)$ given by

$$\alpha(W,Q) = \iint\left(\ln\frac{S(\tau,\nu)}{W(\nu)} + \frac{\pi\tau\nu}{Q}\right)^2 d\tau d\nu, \tag{20}$$

with respect to Q. Equation (20) expresses the square of the L^2-norm of the difference between both sides of (19). The domain of integration is finite in accordance with the band-limited, finite-temporal nature of the seismic data.

Remarks concerning numerical integration

The region of integration, say Ω, must be appropriately selected so as to encompass only the numerically significant part of the time-variant spectrum of the signal. This is necessary to avoid large errors due to division by excessively small numbers. For numerical implementations, it is convenient to consider integrals over rectangular domains. All of this can be accomplished by introducing a characteristic weighting function, χ_Ω:

$$\chi_\Omega(\tau,\nu)=\begin{cases}1 \text{ if } (\tau,\nu)\in \Omega\\ 0 \text{ if } (\tau,\nu)\notin \Omega\end{cases} \tag{21}$$

as a factor in the integrand. For example,

$$\int_\Omega f(\tau,\nu)d\tau d\nu=\int_{\nu_0}^{\nu_1}\int_{\tau_0}^{\tau_1} f(\tau,\nu)\chi_\Omega(\tau,\nu)d\tau d\nu, \tag{22}$$

where f is any integrand with numerically stable support Ω, and Ω is contained in the rectangle $[\tau_0,\tau_1]\times[\nu_0,\nu_1]$. Any positive weighting function can be substituted for χ_Ω at the discretion of the processor. Ideally, this function should decay to zero in a smooth way to avoid spectral ringing.

From now on, we will assume that an appropriate region Ω (or weighting function) has been selected. As such, expression (20) can be written in the form

$$\alpha(W,Q)=\int_\Omega\left(\ln\frac{S(\tau,\nu)}{W(\nu)}+\frac{\pi\tau\nu}{Q}\right)^2 d\tau d\nu, \tag{23}$$

which can be computed according to the prescription (22). Minimizing (23) with respect to Q amounts to solving the following equation for Q:

$$0=\frac{\partial\alpha}{\partial Q}=2\int_\Omega\left(\ln\frac{S(\tau,\nu)}{W(\nu)}+\frac{\pi\tau\nu}{Q}\right)\left(-\frac{\pi\tau\nu}{Q^2}\right)d\tau d\nu. \tag{24}$$

Inspection of (24) reveals the trivial solution, $Q=\infty$, but straightforward calculations lead to the finite value:

$$Q=\pi\frac{\int_\Omega \tau^2\nu^2 d\tau d\nu}{\int_\Omega \tau\nu\ln\frac{W(\nu)}{S(\tau,\nu)}d\tau d\nu}. \tag{25}$$

That this value of Q actually provides a local minimum of $\alpha = \alpha(Q)$ is easy to show by checking that the second derivative of α is positive at this point. Now (25) expresses Q in terms of the unknown wavelet, $W(\nu)$, so a second expression is required. This second relation is derived in the following section.

Step two: least-squares estimate of *W* in terms of *Q*

In the last step, ordinary calculus was sufficient for determining the optimal Q value. Since we are now interested in finding an optimal function, namely $W(\nu)$, we turn to the calculus of variations (see e.g., Marion and Thornton, 1988, or Pearson, 1974).

In order to simplify the notation, we write

$$s = \ln S \text{ and } w = \ln W. \tag{26}$$

Next, consider an arbitrary functional variation, $\delta w = \delta w(\nu)$. Incrementing the unknown function $w(\nu)$ by $\delta w(\nu)$, expression (23) becomes

$$\alpha(w+\delta w, Q) = \int_\Omega \left(s(\tau,\nu) - w(\nu) - \delta w(\nu) + \frac{\pi\tau\nu}{Q} \right)^2 d\tau d\nu \text{, or} \tag{27}$$

$$\begin{aligned} \alpha(w+\delta w, Q) = \alpha(w, Q) - 2\int_\Omega \left(s(\tau,\nu) - w(\nu) + \frac{\pi\tau\nu}{Q} \right) \delta w(\nu)\, d\tau d\nu \\ + \int_\Omega \left[\delta w(\nu) \right]^2 d\tau d\nu. \end{aligned} \tag{28}$$

Notice that, if we can determine a function $w(\nu)$ such that the middle term in (28) vanishes, this same function will minimize $\alpha(w, Q)$ with respect to w. This reduces the problem to solving

$$\int_\Omega \left(s(\tau,\nu) - w(\nu) + \frac{\pi\tau\nu}{Q} \right) \delta w(\nu) d\tau d\nu = 0 \tag{29}$$

for $w(\nu)$. Since $\delta w(\nu)$ is independent of the time, τ, we can compute the time integral in (29), yielding

$$\begin{aligned} \int_{\nu_0}^{\nu_1} \Big\{ \int_{\tau_0}^{\tau_1} s(\tau,\nu)\, \chi_\Omega(\tau,\nu) d\tau - \\ w(\nu) \int_{\tau_0}^{\tau_1} \chi_\Omega(\tau,\nu) d\tau + \frac{\pi\nu}{Q} \int_{\tau_0}^{\tau_1} \tau \chi_\Omega(\tau,\nu)\, d\tau \Big\} \delta w(\nu)\, d\nu = 0. \end{aligned} \tag{30}$$

The ν-integral vanishes for all variations $\delta w(\nu)$, so it follows from the calculus of variations that the function of ν inside the braces must vanish. Thus, upon division by $\int_{\tau_0}^{\tau_1} \chi_\Omega(\tau,\nu)d\tau$, and solving for $w(\nu)$, we have

$$w(\nu) = \frac{\int_{\tau_0}^{\tau_1} s(\tau,\nu)\chi_\Omega(\tau,\nu)d\tau}{\int_{\tau_0}^{\tau_1} \chi_\Omega(\tau,\nu)d\tau} + \frac{\pi\nu}{Q}\frac{\int_{\tau_0}^{\tau_1} \tau\chi_\Omega(\tau,\nu)d\tau}{\int_{\tau_0}^{\tau_1} \chi_\Omega(\tau,\nu)d\tau}. \tag{31}$$

Using (26) to convert back to the logarithmic notation, we arrive at

$$W(\nu) = \exp\left\{\frac{\int_{\tau_0}^{\tau_1} \ln\left[S(\tau,\nu)\right]\chi_\Omega(\tau,\nu)d\tau}{\int_{\tau_0}^{\tau_1} \chi_\Omega(\tau,\nu)d\tau} + \frac{\pi\nu}{Q}\frac{\int_{\tau_0}^{\tau_1} \tau\chi_\Omega(\tau,\nu)d\tau}{\int_{\tau_0}^{\tau_1} \chi_\Omega(\tau,\nu)d\tau}\right\}. \tag{32}$$

The first term in the exponential expresses the time average of $\ln S(\tau,\nu)$, while the second term is both linear in frequency and proportional to the average time for each frequency. Using a bar to denote the time average, (32) can be written more compactly as

$$W(\nu) = \exp\left\{\overline{[\ln S]}(\nu) + \frac{\pi\nu}{Q}\bar{\tau}(\nu)\right\}. \tag{33}$$

Observe that these time averages are functions of frequency. Physically, this result for $W(\nu)$ states that the best least squares logarithmic fit for the wavelet is obtained as the time average of $\ln W(\nu)$, expressed in terms of the model. In other words, had we solved (19) for $\ln W(\nu)$, then computed the time average, we would have arrived at the same solution (33).

Solving for *Q*

Substitution of (33) into the expression (25) for Q yields

$$Q = \pi \frac{\int_\Omega \tau^2\nu^2 d\tau d\nu}{\int_\Omega \tau\nu\left[\overline{[\ln S]}(\nu) + \frac{\pi\nu}{Q}\bar{\tau}(\nu) - \ln S(\tau,\nu)\right]d\tau d\nu}. \tag{34}$$

Finally, solving for Q leads to

$$Q = \pi \frac{\int_\Omega \tau\nu^2\left[\tau - \bar{\tau}(\nu)\right]d\tau d\nu}{\int_\Omega \tau\nu\left[\overline{[\ln S]}(\nu) - \ln S(\tau,\nu)\right]d\tau d\nu}. \tag{35}$$

NUMERICAL EXAMPLE

MATLAB® functions from the CREWES toolboxes were used extensively in developing the code to generate the least-squares estimates (35) and (33) of Q and $W(\nu)$, respectively and to perform a Gabor deconvolution. The details of the Gabor deconvolution algorithm may be found in Margrave and Lamoureux (2001). Figure 1 displays a pseudo-random reflectivity and a nonstationary synthetic trace. The synthetic was built by applying a forward Q operator to the reflectivity, followed by convolution with a 20Hz minimum phase wavelet. The reflectivity has a duration of two seconds, with a sampling interval of 0.002 seconds.

Figure 2 displays the Gabor transform of the reflectivity. The sample points in the time direction (row number) correspond to successive translations by 0.01 seconds of Gaussian window centres. These Gaussian windows have the property that their sum is approximately equal to one over the duration of the synthetic trace, and their half-width (0.1 seconds) has been selected such that this criterion is met. Each row is computed as the discrete Fourier transform of the windowed trace that is centred at the corresponding offset time. In order to obtain sharp spikes, the reflectivity has been modified from its original, uniformly distributed, random sequence. This modification leads to a time series that is no longer uniformly distributed and induces the weak coherency that can be observed along the frequency direction in its Gabor transform. This behaviour is similar to that in real reflection coefficient series, such as those from well logs. Each sequence of coherent peaks, such as those at about 1 second corresponds to a zone of high amplitude in the reflectivity of Figure 1.

The Gabor transform of the logarithm of the absolute value of the synthetic trace is depicted in Figure 3. Since the Q-operator represents an exponential decay surface in time and frequency, its logarithm forms a surface whose level sets (i.e. contours) are hyperbolae, decaying in magnitude according to the product of the time and frequency values. This explains the general decay pattern from the top left toward the bottom right in Figure 3. There is progressive loss of bandwidth and mean amplitude over time.

Figures 4, 5, and 6 illustrate the construction of a weighting function, which is designed to filter out that part of the data falling below machine precision. This weighting function was used in the calculation of the integrals in equations (33) and (35) in the manner illustrated in equation (22). Figure 4 essentially matches the decay pattern of the data, while Figure 5 displays a secondary filter designed to remove edge effects arising from the Gabor transform. The point-wise product of these two filters is shown in Figure 5. This final filter is selected as the weighted characteristic function mentioned above (see *Remarks concerning numerical integration* and equation (22)) to restrict the domain of integration.

The prescriptions of equations (35) and (33) produced an estimated Q value of about 28, slightly greater than the correct value of 25, and the estimated wavelet, whose Fourier spectrum is plotted with that of the original wavelet in Figure 7. The envelope of the output wavelet has roughly the right shape, but some additional smoothing would likely lead to better deconvolution results. The rugosity in the wavelet spectral estimate is a residual effect of the reflectivity and is undesirable.

Essentially, it means that, in the time averages in equation (33), the reflectivity has failed to average to unity. Even a mathematically "white" white function will only average to unity if the average is over an infinite domain. Obviously, the domain available here is very finite.

Figure 8 displays the logarithm of the absolute value of the least-squares model of the data. That is it is calculated as $\ln\left[\left|\hat{w}(\nu)\right|_{est} e^{-\pi\nu\tau/Q_{est}}\right]$ where the subscript *est* refers to the least-squares estimates. As expected, the amplitude decays smoothly, and resembles a smeared version of the display in Figure 3. For this reason we refer to this least-squares model as a *smoothed representation* of the data.

The deconvolution operator is approximately the inverse of $\left|\hat{w}(\nu)\right|_{est} e^{-\pi\nu\tau/Q_{est}}$ combined with the associated minimum-phase spectrum. However, a small positive constant, called a stability factor, is added to $\left|\hat{w}(\nu)\right|_{est} e^{-\pi\nu\tau/Q_{est}}$ prior to inversion to prevent the inversion of small, low-precision, numbers. The magnitude of this deconvolution operator is shown in Figure 9. Cross sections of the input and least-squares model Gabor spectra at time t = 1s, plotted in decibels, appear in Figure 10. The plot clearly illustrates the effect of the stability factor that causes the model to become constant above about 80Hz. Mathematically, the exponential constant-Q operator should give an exponential decay over all frequencies. In Figure 10, this exponential decay is indicated by the linear trend down from about 20Hz to about 70Hz. in the input spectrum. At higher frequencies, the input spectrum begins to level out and depart from this mathematical expectation. In this simulation, which has no added noise, this is due to the limited-precision, floating-point arithmetic employed in our digital calculations. Higher precision computation would lead to agreement over a larger bandwidth, particularly since this stability factor could be made smaller. However, this would only mask the precision problem, which is very real, and is magnified in real seismic data due to the limited precision of seismic recording.

Figure 11 shows the spectra of the original reflectivity and the Gabor deconvolution result. Whitening has been limited to below 125Hz – half of Nyquist, by a stationary bandpass filter. The two spectra agree quite well over the whitened band though discrepancies increase with increasing frequency. Ultimately, the precision problem mentioned in the previous paragraph limits degree of whitening that can be achieved. Since the level sets of the constant-Q operator are the hyperbolae, $\tau\nu = \text{constant}$, then the maximum possible whitening will be time-variant. Finally, Figure 12 compares the original reflectivity, the synthetic seismogram, and the Gabor deconvolution result. The reflector locations are well correlated, although the amplitudes are somewhat mismatched. The increasing error at later times might be attributable to the fact that only a stationary bandpass filter was applied to the deconvolved trace in the time domain. Other discrepancies are probably due to the errors in the wavelet estimate that, as discussed previously, are attributable to reflectivity information failing to average out in the estimate.

CONCLUSIONS

A derivation, to first order, of a time-variant spectral model for the Gabor transform of a constant-Q-attenuated seismic trace was presented. Using ordinary calculus, together with the calculus of variations, the model was fitted to the data in the least-squares sense. Consequently, estimates for both Q and the stationary part of the wavelet were obtained, and thus an estimate of the nonstationary, Q-attenuated wavelet. The theory was then numerically evaluated via an algorithm for the Gabor deconvolution of a synthetic, Q-attenuated seismic trace. The illustrated example used an exceptionally low input Q-value, yet returned promising initial deconvolution results. These favourable results, clearly reinforced by the fact that our model includes the convolutional model as a special case, strongly motivate further research in this direction.

FURTHER RESEARCH

Several parameters in the code require adjustment whenever the input trace changes, so it would be advantageous to automate this parameter selection as much as possible. Certain edge effects arise from the Gabor transformation step and the weighting function, and these need to be suppressed. Either would lead to a more robust estimate of the wavelet, and hence a better deconvolution. The possibility of noise reduction via the least-squares residual error should be investigated. A smoother wavelet estimate should either be imposed after-the-fact or, ideally, via a smoothness constraint in the inversion. The effect of the Gabor window size and increment needs more investigation. Reflectivity information such as a better model for whiteness or an available well log needs to be incorporated. An allowance for a time-variant Q estimate should be investigated. Finally, the algorithm needs to be optimized for speed as well as robustness.

ACKNOWLEDGEMENTS

We thank the sponsors of the CREWES Project for their generous financial support of our research. Other support came from NSERC and MITACS. Much of this work has evolved from a weekly seminar on Gabor Analysis, led by the POTSI project, which the authors have participated in over the past spring and summer sessions at the University of Calgary. (POTSI, or *Pseudodifferential Operator Theory in Seismic Imaging*, is a collaborative research project between the University of Calgary departments of Mathematics and Geophysics , supported by MITACS, Imperial Oil, CREWES, and NSERC.) Aside from the authors, Victor Iliescu and Kris Vasudevan participated in these seminars and provided valuable discussion. Thanks also go to Glenn Morgan for helpful suggestions and proofreading.

REFERENCES

Aki, K. and Richards, P.G., 1980, Quantitative seismology, theory and methods: W.H. Freeman and Company, Volumes 1 and 2.

Feichtinger, H.G. and Strohmer, T., 1998, Gabor analysis and algorithms, theory and applications: Birkhauser.

Gabor, D., 1946, Theory of communication: J. IEEE (London), **93**, 429-457.

Margrave, G.F., 1998, Theory of nonstationary linear filtering in the Fourier domain with application to time-variant filtering: Geophysics, **63**, 244-259.

Margrave, G.F. and Ferguson, R.J., 1998, Nonstationary filters, pseudodifferential operators, and their inverses: CREWES Research Report, Volume 10.
Margrave, G.F. and Lamoureux, M.P., 2001, Gabor deconvolution: CREWES Research Report, this volume.
Marion, J.B. and Thornton, T.T., 1988, Classical dynamics of particles and systems: Harcourt Brace Jovanovich.
Pearson, C.E., 1974, Handbook of applied mathematics: Van Nostrand.
Sheriff, R.E. and Geldart, L.P., 1982, Data-processing and interpretation: Cambridge University Press, Volume 2.

FIGURES

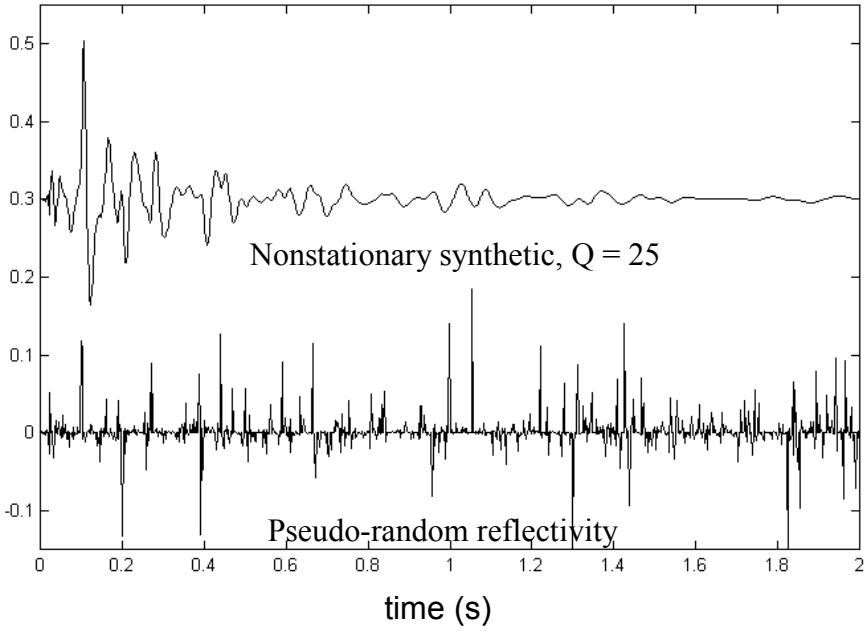

FIG. 1. A pseudo-random reflectivity (lower) and a nonstationary synthetic (upper) generated with an attenuation factor of 25.

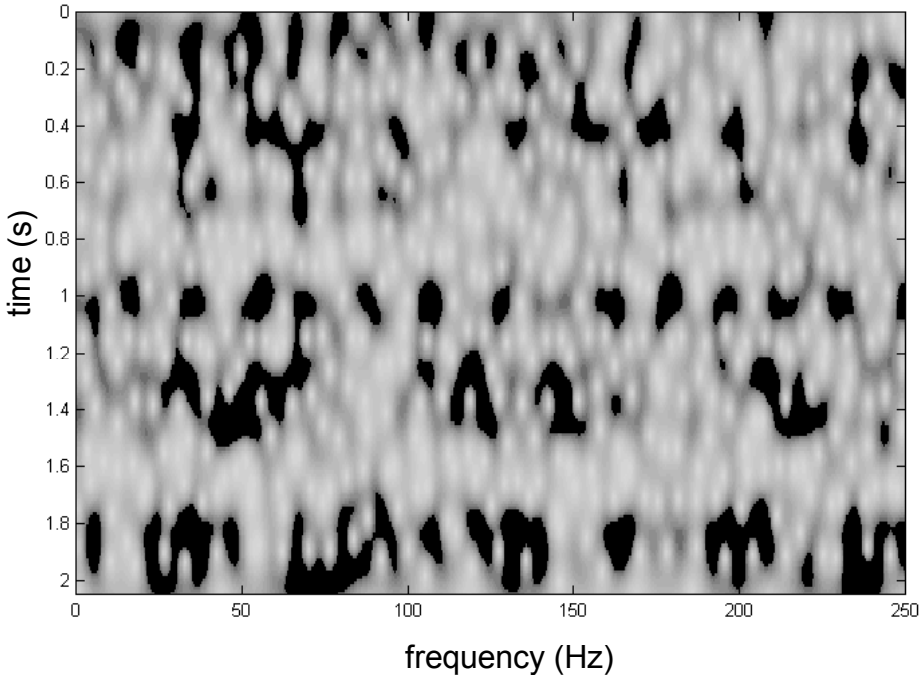

FIG. 2. Gabor spectrum of the pseudo-random reflectivity of Figure 1.

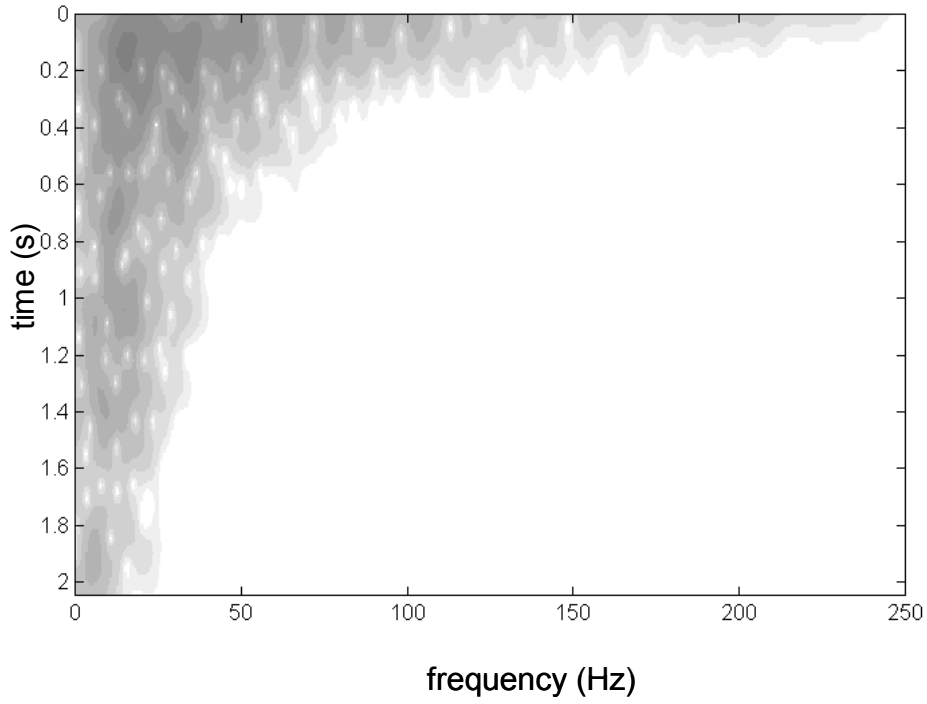

FIG. 3. Logarithm of absolute value of Gabor transform of the synthetic trace of Figure 1.

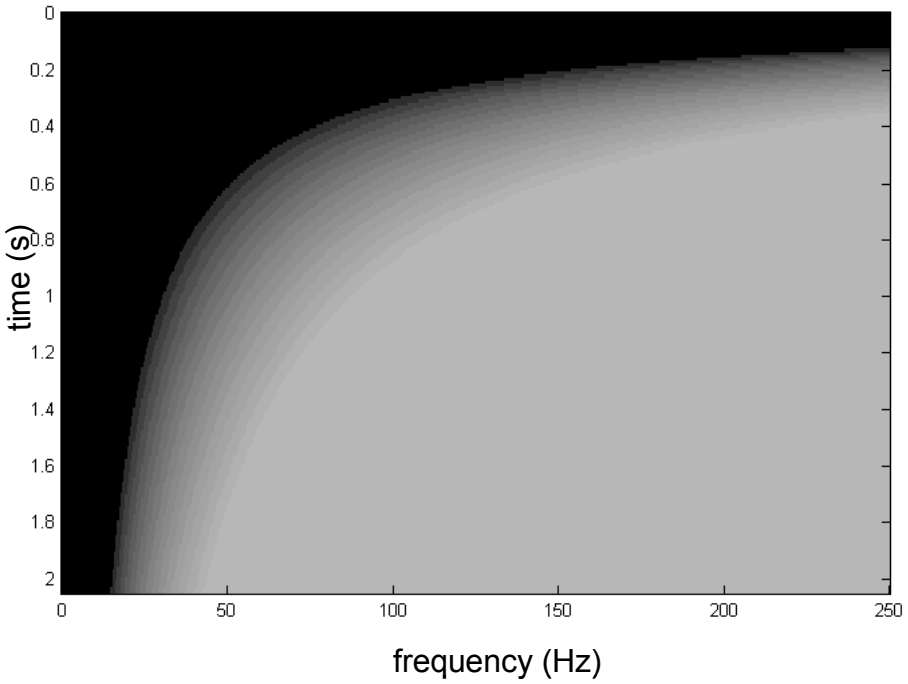

FIG. 4. Filter design for first stage in weighting the Gabor spectrum of the synthetic trace according to the numerical precision of the data.

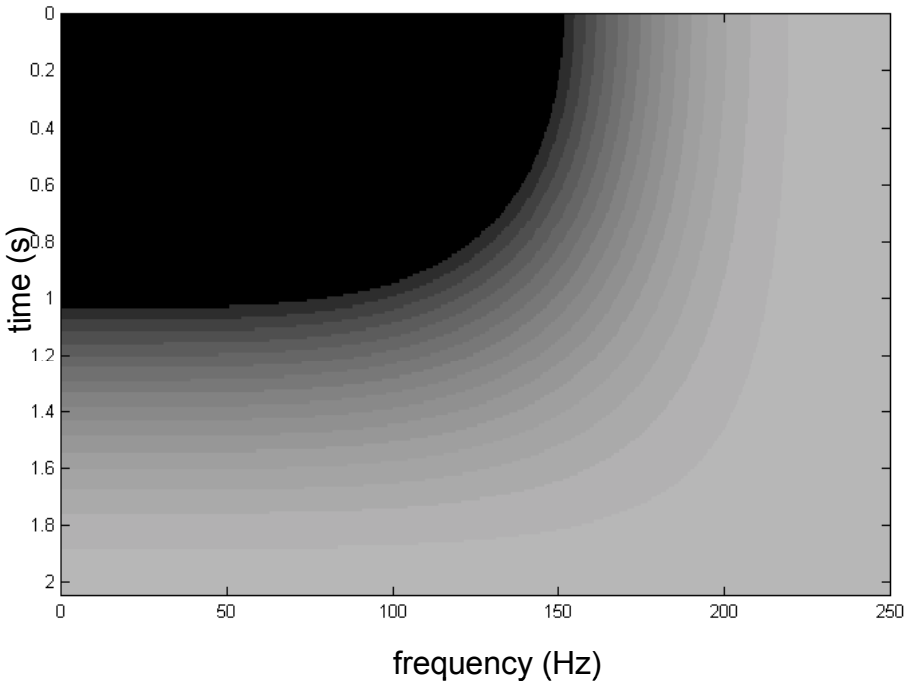

FIG. 5. Secondary filter designed to dampen edge effects resulting from the Gabor transformation of the synthetic trace.

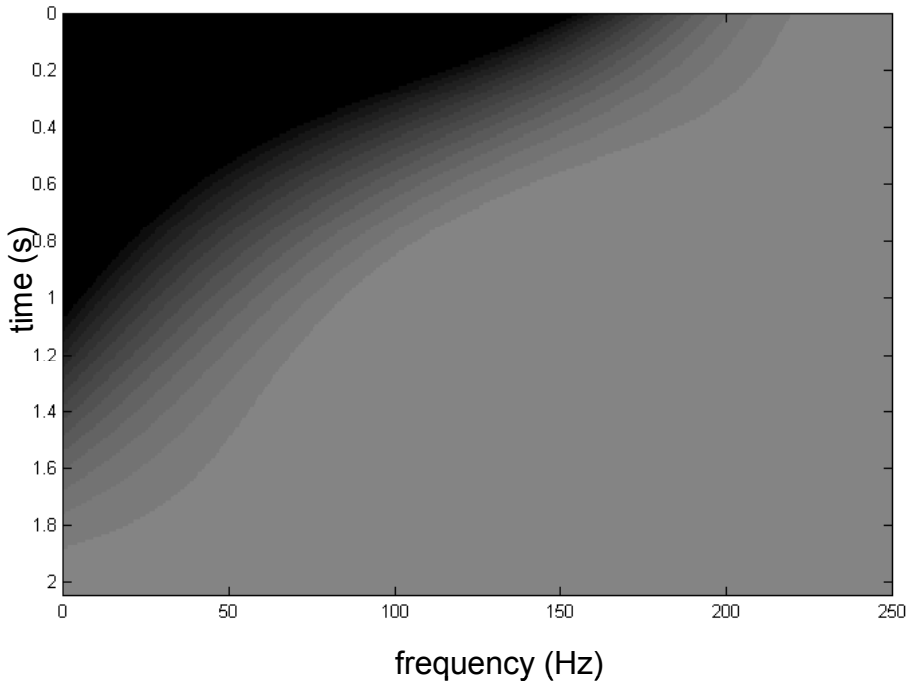

FIG. 6. The weighted domain of integration resulting from the point-wise product of the filters in the previous two Figures.

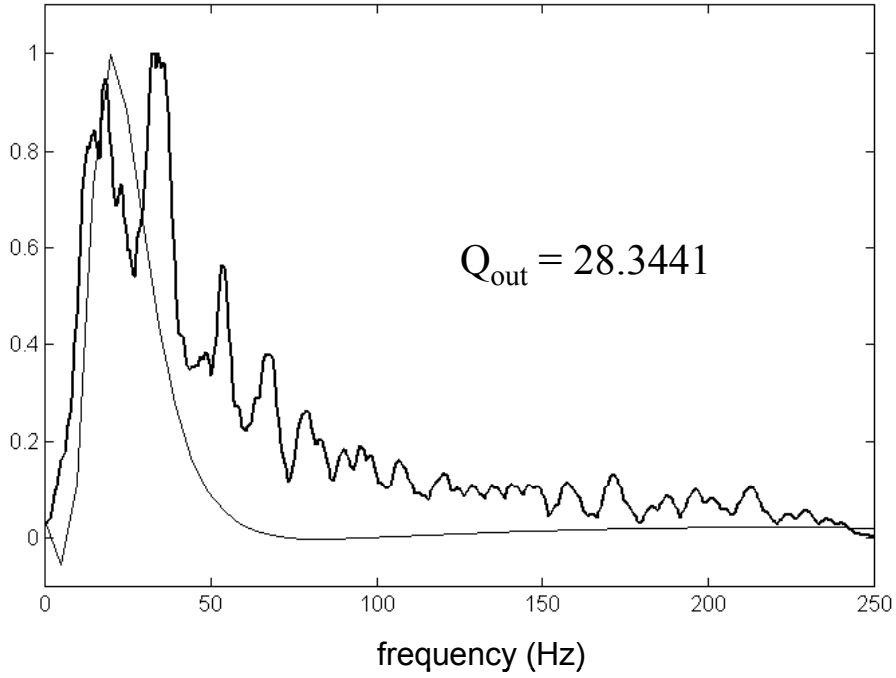

FIG. 7. Amplitude spectra of the input wavelet (grey) and the output wavelet (black).

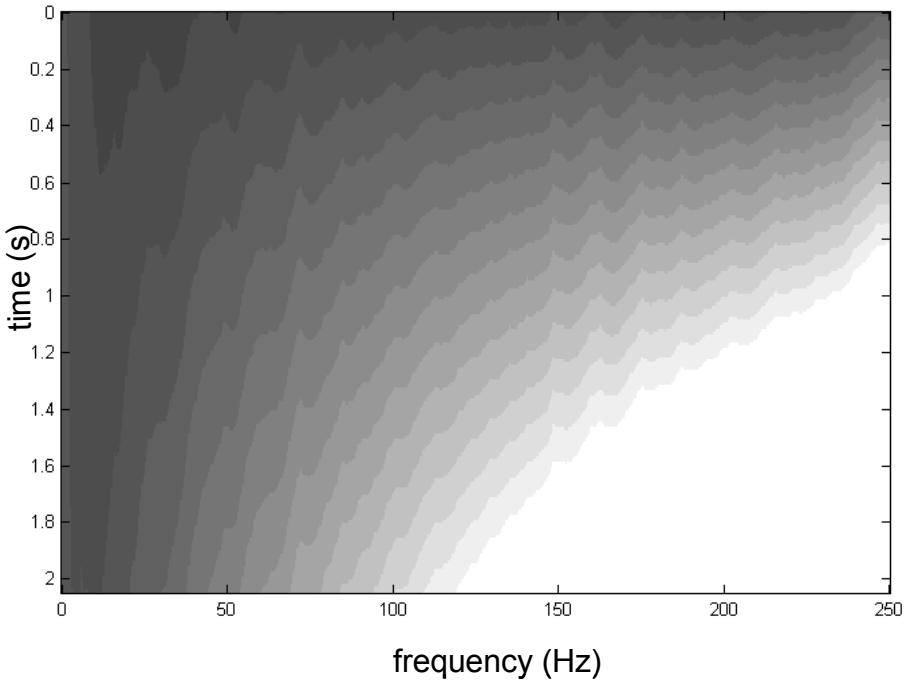

FIG. 8. The logarithm of the absolute value of the smoothed spectrum. The output for the attenuation factor is $Q_{est} \approx 28$.

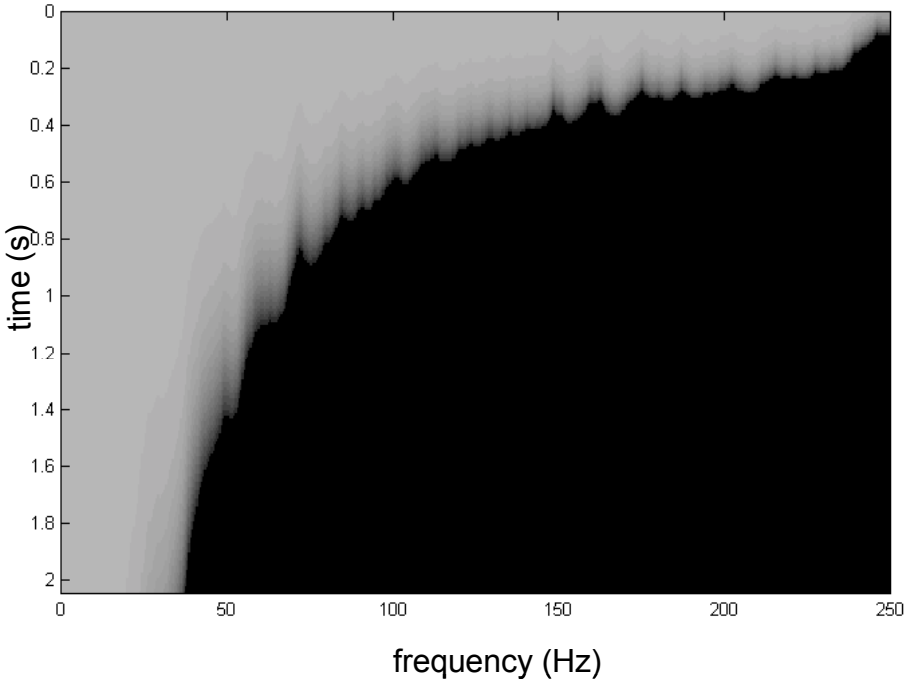

FIG. 9. The magnitude of the deconvolution operator that is point-wise reciprocal of the exponential of the previous figure.

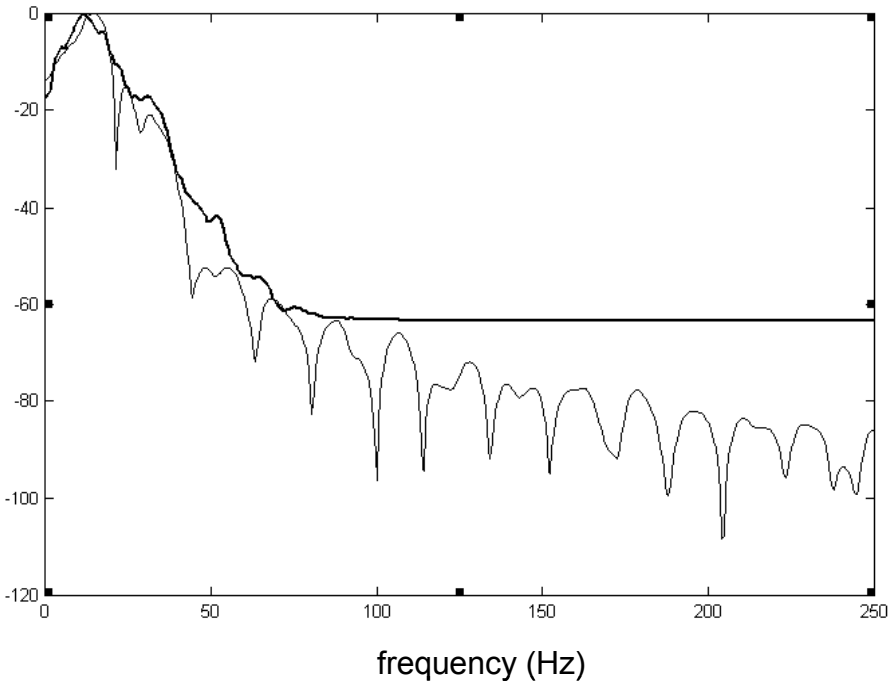

FIG. 10. Cross sections of the input (grey) and smoothed (black) Gabor spectra at time t = 1s, plotted in decibels. A stability factor was added to the smoothed spectrum to avoid division by excessively small numbers.

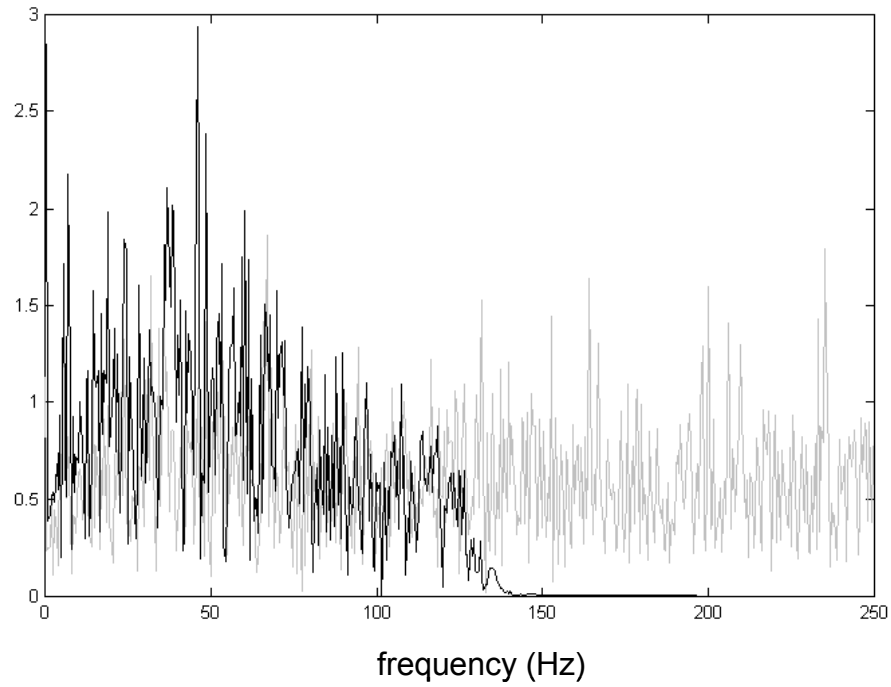

FIG.11. Fourier spectra of original reflectivity (grey) and Gabor deconvolution result (black).

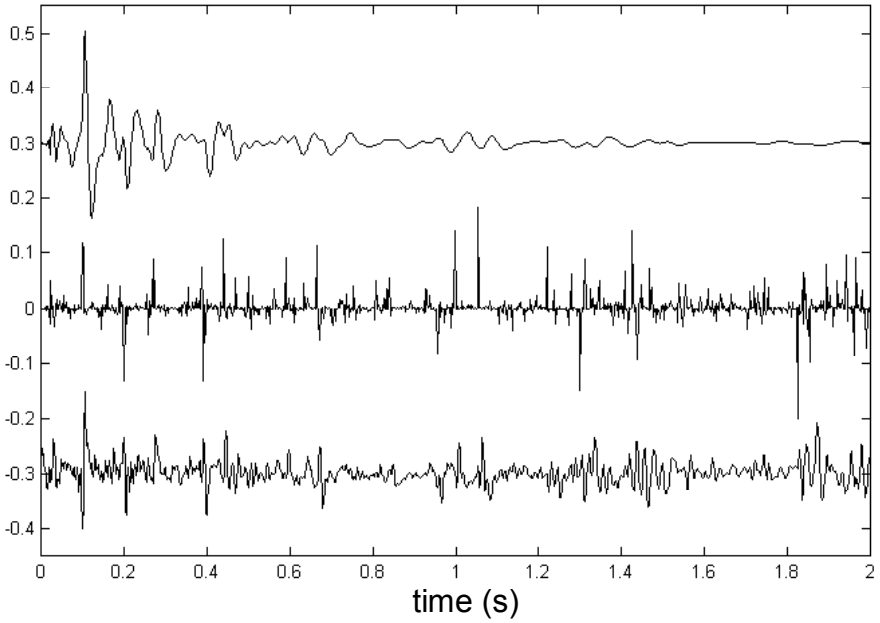

FIG. 12. The nonstationary synthetic (upper), pseudo-random reflectivity (middle), and the Gabor deconvolution result (lower).